MANUFACTURING AND FLEXURAL TESTING OF COMPOSITE BRAIDED HOCKEY STICKS WITH EMBEDDED FIBER OPTIC SENSORS

M. Selezneva*, C. Poon*, A. Nakai**,
X. Gu*, Z. Fawaz*, K. Behdinan*, V. Kulisek***
*Ryerson University, Toronto Canada
350 Victoria Street, Toronto, Ontario, Canada M5B 2K3
**Kyoto Institute of Technology, Kyoto Japan
Matsugasaki, Sakyo-ku, Kyoto 606-8585 JAPAN
*** Czech Technical University, Prague Czech Republic
Technicka 4, 166 07, Prague 6, Czech Republic
M. Selezneva: mselezne@ryerson.ca

SUMMARY

This paper outlines the manufacturing process for braided composite hockey stick with embedded fiber optic sensors. The effect of the braiding parameters on the residual strains and resultant stiffness is investigated, and the overall performance of FBGs for such applications is assessed.

Keywords: braided composites, manufacturing processes, fiber optic sensors, fiber Bragg grating (FBG), residual strain, stiffness measurement

INTRODUCTION

Fiber reinforced composite materials are widely used in aerospace, automotive and sporting goods industries. A lot of current research is aimed towards development of effective techniques for in-situ cure and health monitoring of composite materials, which would allow for better control of the manufacturing processes and provide viable information on the integrity of the structure throughout its lifetime. Another important research focus is on automation of the fabrication process which is critical for mass production.

Fiber Optic Sensors

Conventional techniques used for strain measurements involving strain gauges and extensometers are not suitable for health monitoring of in-service structures as they are difficult to mount onto general parts without affecting their usage. They are also limited to surface strain measurements, which could be significantly different from the internal strains. Fiber optic sensors are attractive for internal strain measurements as they are compatible with common resins, allow for multiplexing and can be introduced into the

material without weakening it because of their small size (250 μm). As a result, the utilization of fiber optic sensors has gained a lot of interest over the last decade.

A fiber Bragg grating (FBG) is a periodic variations of the index of refraction inscribed or written along a section of a silica optical fiber by exposing it to an intense UV-laser light. The gratings acts as a filter, reflecting wavelengths close to the Bragg wavelength λ_B, while transmitting other wavelengths [1]. Bragg wavelength is defined by Eq. 1, where n_{eff} is the effective index of refraction and Λ is the pitch of the grating.

$$\lambda_B = 2n_{eff}\Lambda \tag{1}$$

From Eq. 1 it is evident that any change in an index of refraction or a grating pitch leads to a shift of the Bragg wavelength. This relation can be further expanded to include the effect of strain, temperature and fiber properties on the Bragg wavelength, as described by Eq. 2 [1],

$$\Delta\lambda_B = 2n\Lambda\left[\left\{1-\left(\frac{n^2}{2}\right)\left(P_{12}-\upsilon\left(P_{11}+P_{12}\right)\right)\right\}\varepsilon+\left\{\alpha+\frac{\left(\frac{dn}{dT}\right)}{n}\right\}\Delta T\right] \tag{1}$$

where P_{ij} are the Pockel's coefficients of the stress-optic sensors, ν is the optical fiber Poisson's ratio, ε is the applied strain, α is the coefficient of thermal-expansion of optical fiber and ΔT is the change of temperature.

Equation 2 can be divided into the two parts: an influence of a strain load and an influence of a temperature. The FBG sensor's strain response arises due to both the physical elongation of the sensor (change of a grating pitch) and the change in fiber index due to photo-elastic effects, and can be expressed by factor f,

$$f = 1-\left(\frac{n^2}{2}\right)*\left(P_{12}-\upsilon\left(P_{11}+P_{12}\right)\right) \tag{3}$$

Based on the typical properties for a fiber optic as given by Tao et al [2] the factor f has an approximate value of 0.800. Thus, under a constant temperature conditions Eq. 2 can be transformed into a strain-wavelength relationship, as presented by Eq. 4.

$$\varepsilon = \frac{\Delta\lambda_B}{f.\lambda_B} = \frac{1}{0.8}\frac{\Delta\lambda_B}{\lambda_B} \tag{4}$$

Braided Composites

Braiding process allows for fabrication of seamless tubular components, the main advantage of which over their unidirectional and woven counterparts is the fiber continuity. The interlacing of continuous fibers throughout the entire length of the component promotes good load distribution, giving braided components superior fatigue

and impact resistance. The resultant mechanical properties depend on the structure of the braided material [4], with the most influential parameters being the braid angle and the middle-end fibers (MEFs). Schematic representation of a braided tube is shown in Figure 1. Furthermore, the fabrication process can be easily automated and the process parameters can be adjusted to obtain the desired braid structure.

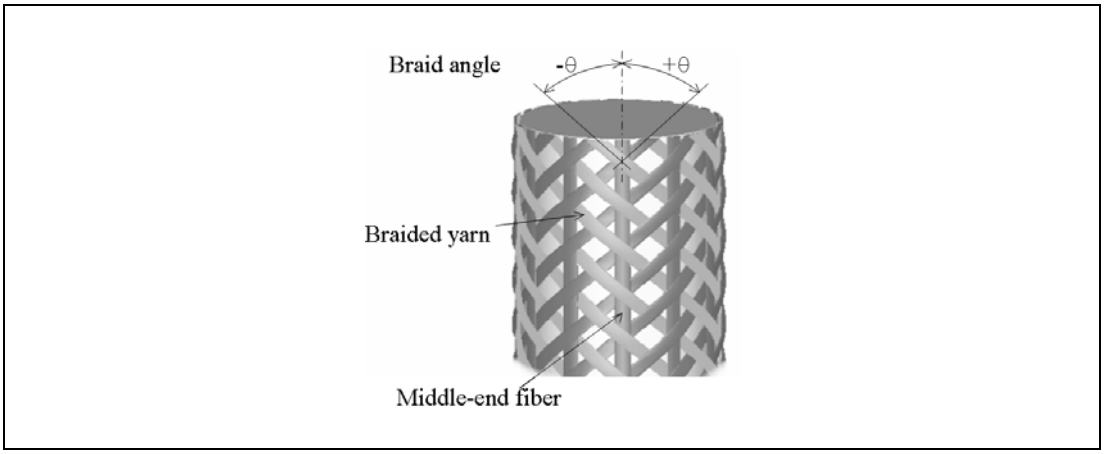

Figure 1, Geometry of a tubular braided specimen [4].

The purpose of this study was to characterize the flexural properties and manufacturing residual strains of the braided specimens with respect to the braid angle and the MEFs with FBG sensors embedded in the composites. We describe the braiding manufacturing process of carbon fiber reinforced polymer (CFRP) for a hockey stick and the embedding process for FBG sensors. We also present the performance of the hockey sticks under four-point bending tests.

MANUFACTURING AND TESTING

Fiber Optic Sensors

Fiber optic sensors were written on a hydrogen-loaded SMF-28 fiber by using a phase mask method. A more detailed description of the method can be found the paper by Lu et al. [3]. The laser used was a collimated KrF excimer laser (Lumonics, model PM 844) that emits laser pulses at 248 nm with energy of 260 mJ at a repetition rate of 30 pulses per second. Once the gratings were written, they were coated with protective polyamide coating, and annealed at 150°C for 15 hours to ensure their long-term stability. There were three gratings of 3 mm in length written on each fiber optic array placed 203 mm (8 in) apart. Gratings had wavelengths in the range of 1530 to 1550 nm, reflectivity of 80 to 90% and a -3 dB bandwidth of ~0.3 nm. The FBG section of the fiber, coated with polyimide of 160 μm in diameter is much thinner than the rest of the fiber of 250 μm diameter polyacrylate coating.

We conducted a beam bending experiment in order to compare the strain readings between our FBG sensor and a conventional strain gauge. A polyimide coated FBG sensor was surface mounted on one side of an aluminum bar while a strain gauge was

attached to the other side using epoxy. The FBG was under compression and the strain gauge was under tension in the test. The aluminum bar was horizontally mounted with one end fastened and the other end left free. The load was applied to the free end of the cantilever beam at a displacement of 1.27 mm (0.05 in) per step up to a maximum displacement of 15.24 mm (0.6 in). For each displacement, strain readings from both FBG and strain gauge were recorded, and plotted in Figure 2. An excellent correlation between the two sets of strain readings was demonstrated with a resulting overall error of less than 0.5% in the strain measurements.

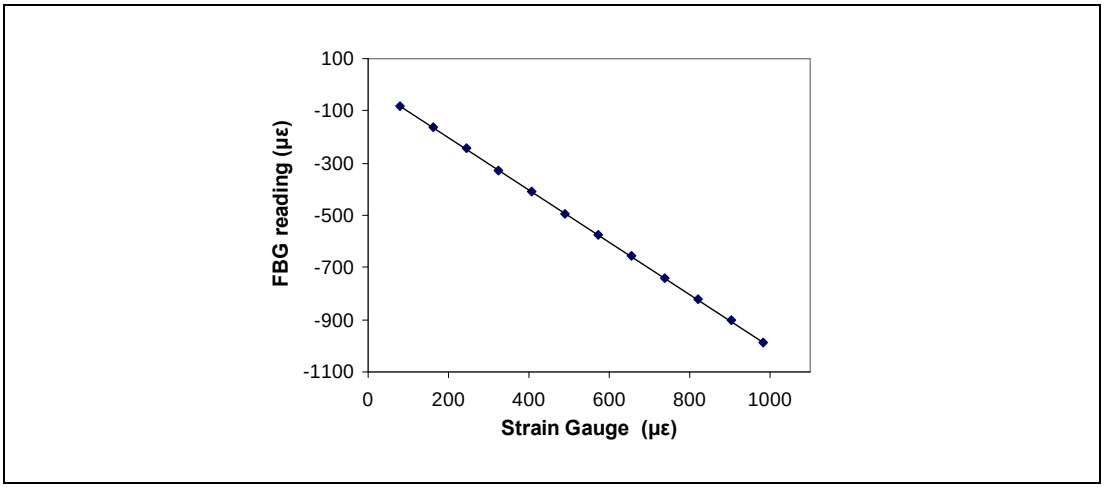

Figure 2, Calibration curve between a strain gauge and a FBG sensor.

Braided Specimens

Three specimen configurations were considered, 30° braid angle, 45° braid angle and 45° braid angle with 12 MEFs. These specimens were fabricated by braiding carbon pre-preg yarn around a rectangular mandrel (24 x 16 mm) by using a tubular braiding machine (Murata Machinery, Ltd.). The carbon pre-preg yarn was supplied by Nippon oil corporation, and had 35wt% resin impregnation ratio consisting of carbon yarn (TORAYCA T700-6k) and modified epoxy (Nippon oil corporation). Specimens with a 45° braid angle had two layers, with the fiber optic cable placed between them. Whereas, specimens with a 30° braid angle had three layers, in order to ensure sufficient stiffness for post-cure handling, with the fiber optic cable placed between the second and third layers. Protective tubing was placed on the non-embedded portion of the fiber optic while extending 10 mm (0.4 in) into the braided section to protect it from breakage. After braiding, the preform was wrapped with tape, clamped with cold plates, to achieve rectangular cross-section, and cured in the oven at 130°C for 2 hours and subsequently at 150°C for 1 more hour.

Four-Point Bending Test

The flexural modulus of elasticity of the specimens was determined by performing a static four-point bending test. Specimens were positioned to have a total support span of

609.6 mm (24 in) and a load span of 203.2 mm (8 in). Loading was applied with precision weights (Hi Tech) in the increment of 5 N (1.12 lb) up to a maximum load of 180 N (40.47 lb). Rollers with a diameter of 25.4 mm (1 in) were used to achieve line loading at the load application and the support locations. A strain gauge (Vishay Micro-Measurements EA-06-250AE-350) was placed axially in the center of the specimen, which corresponded to the constant strain section, on the same side as the FBGs sensors. Strain readings were monitored with a strain gauge and FBG sensors simultaneously, for which P3 Strain Indicator (Vishay Micro-Measurements) and Si425 Interrogator (Micron Optics) were employed, respectively. Each specimen was tested twice to record sensor readings in both tension and compression. Refer to Figure 3 for the schematic representation of the apparatus set up and sensor locations.

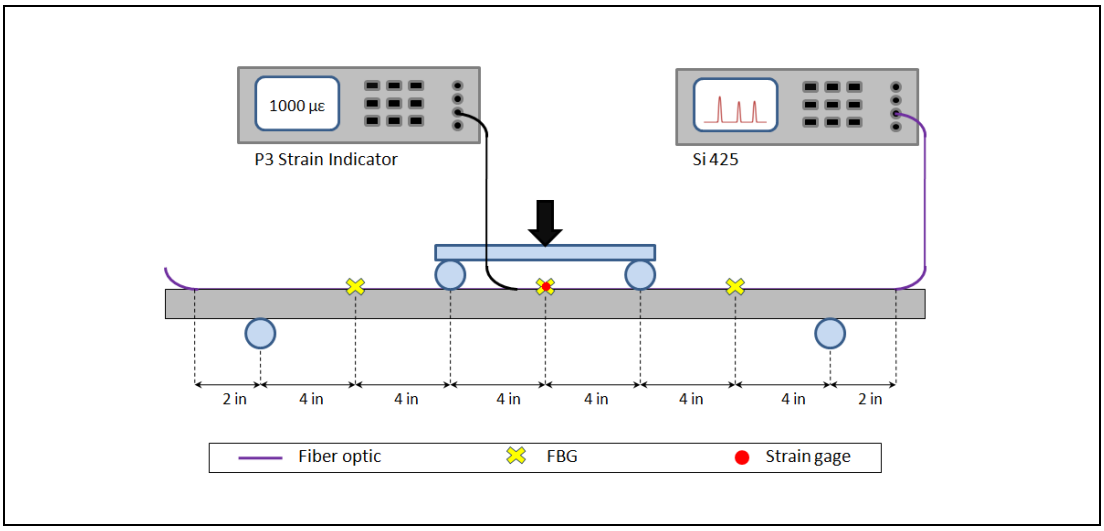

Figure 3, Schematic representation of the apparatus set up and sensor locations.

RESULTS

Manufacturing

At the outcome of the manufacturing process 8 out of 10 fiber optic cables were embedded successfully as shown in Table 1. Figure 4, shows the photographs of three specimen types that were fabricated. It should be mentioned, however, that it was originally desired to automate the embedding process of the fiber array by braiding them in longitudinally as MEFs. It was found that fiber optics could not be braided as originally planned, because the area with the grating could not sustain the shear stresses associated with the 90º bending of the fiber as its orientation changed from the radial to the axial directions, depicted in Figure 5. The arrows in Figure 5 identify the axial direction of the specimen and the radial yarn, with arrows pointing at the locations of high shear stress. Thus, the embedding procedure had to be modified to prevent the grating from breaking, so instead of being braided-in as a MEF, fiber optics were manually laid onto the specimen before braiding the outer layer.

Table 1, Summary of the braiding geometries considered, results of the embedding process and total residual strains.

Braiding Geometry	Number of Specimens Made	Successful Embedding	Average Residual Strain (με)
45°, no MEF	4	3 out of 4	1147.5
45°, with 12 MEFs	3	2 out of 3	1801.0
30°, no MEF	3	3 out of 3	2634.0

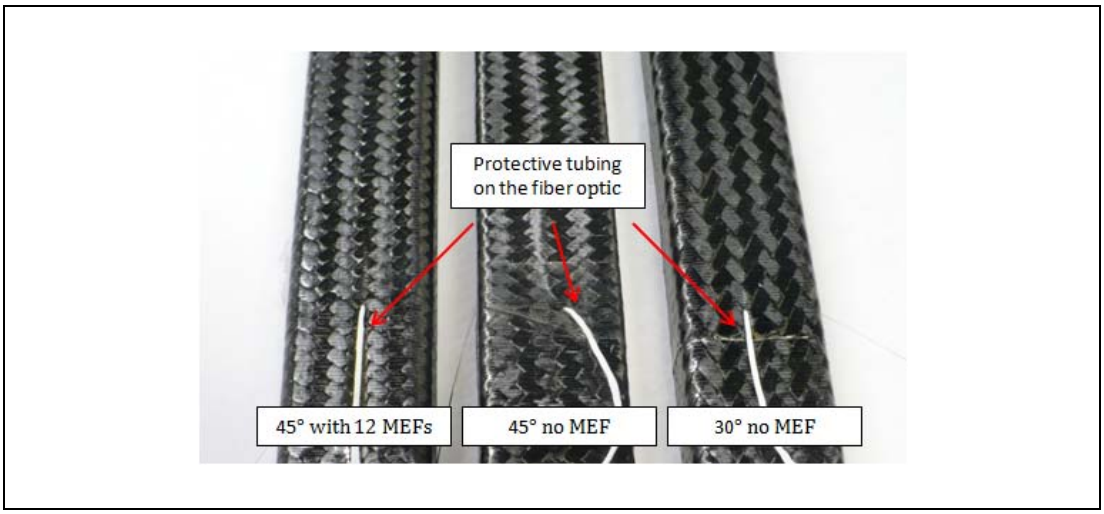

Figure 4, Image of the three types of specimens manufactured and the protective tubing on the fiber optic.

A trial specimen was made by braiding an optical fiber without any grating in place of the MEF. At the end of the manufacturing process the optical fiber was able to transmit light, thus, indicating that it was not damaged. This signified the possibility to automate the embedding process of the fiber optics; however, the problem of braiding-in a fiber with gratings remains to be addressed. The exposure of the fiber optic to laser light during the writing process weakened the grating area. Hence, a lower dosage or pulse energy of the laser could be used to minimize deterioration of the fiber strength. Also, a polyimide coated fiber can be used to make the fiber sensor array, so that the grating will have the same diameter as the rest of the fiber. This would eliminate the areas of high stress concentrations due to an abrupt diameter change. Alternatively, a braiding machine with a smaller transition angle β can be used to decrease the shear stress and prevent the grated area from breaking, see Figure 6.

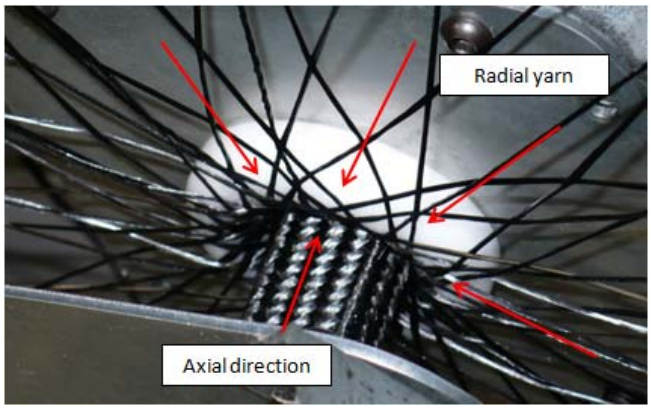

Figure 5, Image showing the bending of the radial yarn as it is braided onto a mandrel. Arrows show the axial and radial direction of the yarn.

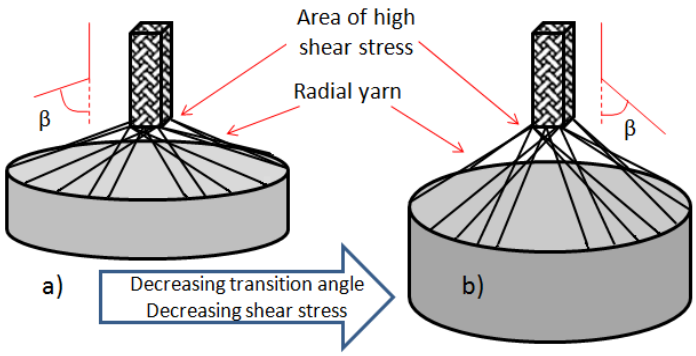

Figure 6, Schematic of a braiding machine with a) high transition angle β and b) low transition angle β.

FBG Spectrums

A definite shift in the FBG wavelength was observed when comparing the spectrum prior to and after manufacturing, as shown in Figure 7. An optical spectrum analyzer (Ando, model AQ 6317) was used. The power of the signal was scaled for the ease of visual comparison because different light sources were used to capture the spectrum, which only affected the intensity of the measured signal and not its profile. From Figure 7, it is evident that there was an intensity drop (comparing peaks of the same spectrum) and chirping of the signal, associated with strain variation along the length of the grating due the specimen microstructure. Figure 7, shows spectrums of a 45°, 12 MEFs specimen, similar observations were made with other specimen types. The shift in the Bragg wavelength was then used to calculated residual strains using Eq. 4.

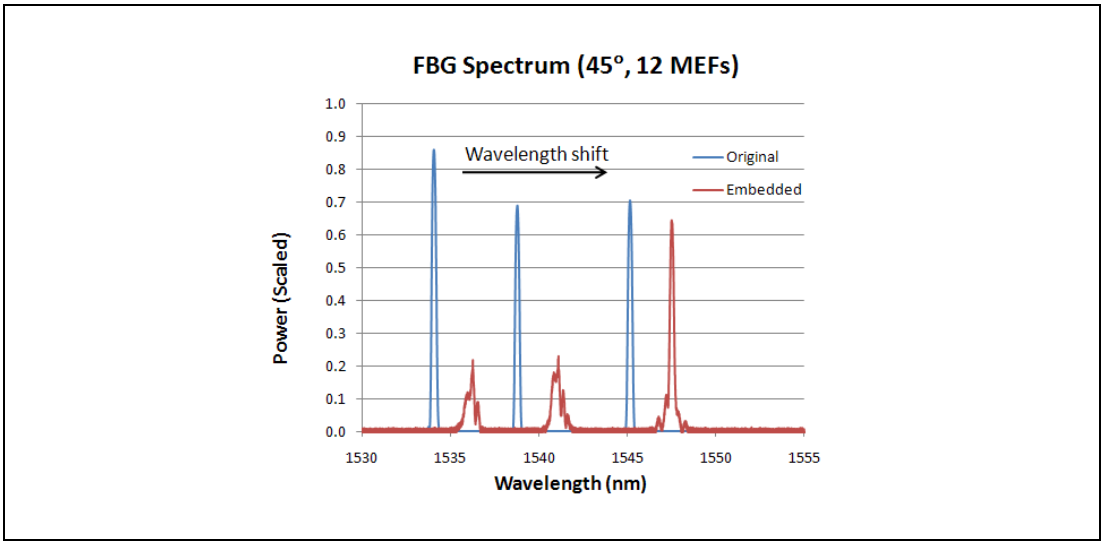

Figure 7, Comparison of spectrums of a 45°, 12 MEFs specimen prior to and after manufacturing.

Residual Strains

The values of the average residual strains measured for the three specimen types are summarized in Table 1**.** From these results, it is evident that the residual strains are depended on the braid angle and the MEFs, in fact the residual strain increased when going from the case of 45º braid angle, to 45º with 12 MEFs to 30º. This dependency could be explained by the fact that, whereas CTE of the epoxy resin is an isotropic property, the CTE of the carbon fiber is anisotropic, which in turn arises from the anisotropy in the fiber stiffness. Since, the longitudinal component of the carbon yarn in the specimen, increases with decreasing braid angles and with the presence of MEFs, the resultant longitudinal tensile residual strain also increases. Similar dependency between the carbon yarn angles and the residuals strains in the longitudinal and the transverse directions have been reported for unidirectional, cross-ply and braided laminates [5, 6, 7].

The combined thermal properties of the carbon fiber (small negative CTE) and epoxy (large positive CTE) yield a small positive CTE of the specimen. This leads to a smaller overall contraction of the specimen during cooling in comparison to the initial unconstrained expansion during heating, thus resulting in tensile residual strains. Similar results were presented by Castro et al. [8] when measuring axial strain in unidirectional carbon epoxy laminates.

Flexural Modulus

The readings from the strain gauges and FBG sensors were used to plot the force-strain relation for the specimens subject to the four-point flexural loading. The slope of the force-strain plot was translated to flexural modulus of elasticity by applying the flexure formula, refer to Table 2. These results indicate that flexural stiffness increased with decreasing braid angle and the addition of the MEFs. Such results were anticipated since

the flexural modulus in the longitudinal direction is strongly influenced by the anisotropic properties of the carbon fiber. Similar results were reported by Ohtani et al. [4] in which case tubular braided carbon-epoxy specimens with the braid angle ranging from 30º to 60º had the respective flexural stiffness ranging from 40.1 GPa to 10.8 GPa.

Table 2, Summary of the braiding geometries considered, total residual strains, and the flexural modulus determined by strain gauges and FBG.

Braiding Geometry	Flexural Modulus Strain Gauge (GPa)	Flexural Modulus FBG (GPa)	Difference (%)
45º, no MEF	12.07	11.77	2.4
45º, with 12 MEF	24.70	25.17	1.9
30º, no MEF	31.63	31.19	1.4

An example of the force-strain relation measured with a strain gauge and FBG sensors is presented in Figure 8. From this plot it is evident that for a given load applied the strain reading of the strain gauge is higher than that of the centered FBG. This result was anticipated since the strain gauge was placed farther away from the neutral axis. The strain measurements taken with off-centered FBGs agreed well with each other, but were lower than those taken with the centered FBG due to the loading conditions, see Figure 3. Overall, modulus calculated from the measurements taken with the strain gauges and FBGs sensors were found to be in a close agreement with each other, with the difference being less than 2.5 %. These results further demonstrated the effectiveness of embedded FBGs for in-situ strain measurements.

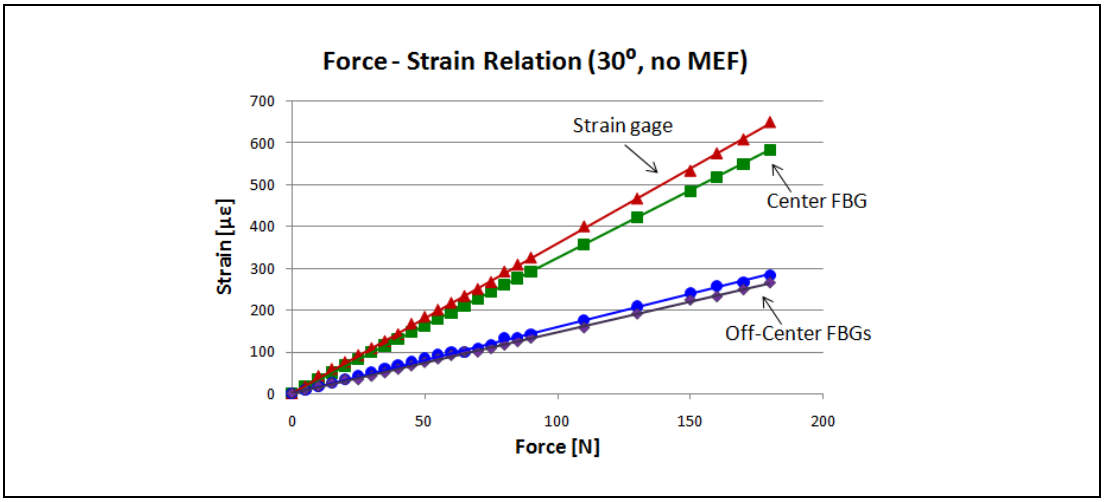

Figure 8, Force-strain relation as measured with a strain gauge, centered FBG sensor and two off-center FBG sensors.

CONCLUSION

This paper discussed the manufacturing process used to fabricate braided hockey sticks with embedded fiber optic sensors. The subsequent analysis showed that residual manufacturing strains and flexural stiffness increase with the presence of MEFs and with a decreasing braiding angle. Such dependency is explained by the anisotropic nature of the specimens. Further modifications to the original manufacturing process were proposed to enable automation of the embedding process. These suggestions include using a braiding machine with a lower transition angle, and using a polyimide coated fiber optic and a lower dosage or pulse energy laser to write a grating. Overall, results of the manufacturing process and the four-point bending test indicated that FBG sensors can be used for in-situ strain monitoring.

ACKNOWLEDGEMENTS

We would like to thank the Office of International Affairs at Ryerson University and the NSERC Discovery Grant for providing the financial support required to undertake this project and travel to Japan to manufacture the specimens. We would also like to extend our acknowledgements to Peter Bradley, who helped to set up the test apparatus and conduct the tests.

References

1. A.D. Karsey, M.A.Davis, J. H. Patrick et al., “Fiber Grating Sensors,” Journal of Lightwave Technology, Volv. 15, no. 8, 1997.
2. X. Tao, L. Tang, W. Du and C. Ad Choy, “Internal strain Measurement by Fiber Bragg Grating Sensors in Textile Composites,” Composite Science and Technology, Vol. 60, 2000.
3. H. Lu, R. Hussain, M. Zhou and X. Gu, “Fiber Bragg Grating Sensors for Failure Detection of Flip Chip Ball Grid Array in Four-Point Bend Tests,” IEEE Sensors Journal, 2008.
4. A. Ohtani and A. Nakai, “Fiber Architecture and Mechanical Properties of Braided Composite Tubes”, Proceedings of the Sixth Canada-Japan Workshop on Composites, Toronto, Canada, 2006.
5. H.-K. Kang, D.-H. Kang, C.-S. Hong et al., “Monitoring of Fabrication Strain and Temperature during Composite Cure using Fiber Optic Sensors”, Proceedings of the 6th Annual Internation Sympsium on NDE for Health Monitoring and Diagnostics, Newport Beach, USA, 2001.
6. R. de Oliveira, S. Lavanchy, R. Chatton et al., « Experimental Investigation of the Effect of the Mould Thermal Expansion on the Development of Internal Stresses during Carbon Fiber Composite Processing”, Composite: Part A, Vol. 39, 2008.
7. K. Jung and T. J. Kang, “Cure Monitoring and Internal Strain Measurement of 3-D Hybrid Braided Composites using Fiber Bragg Grating Sensor”, Journal of Composite Materials, Vol. 41, No. 12, 2007.

8. A. S. Castro, R. Y. Kim and J. D. Russell, " In Situ Monitoring of Residual Strain Development During Composite Cure", Polymer Composites, Vol. 23, No. 3, 2002.

Back to Programme *Back to Topic* *Next Paper*